Structural Durability & Health Monitoring

Tech Science Press

https://doi.org/10.32604/sdhm.2026.079184

ARTICLE

Experimental and Numerical Investigation of Steel Frame-UHPC Composite Deck for Construction Trestles

Wu Yang[1], Quan Xu[1], Zhimin Zhou[2], Mingtao Ye[3] and Shaohua He[3,*]

[1]CCCC Changsha Construction Co., Ltd., No. 1 Jinxingbei Road, Wangcheng District, Changsha, China
[2]Guangdong Guansheng Civil Engineering Technology Co., Ltd., No. 1025, Huateng Road, Panyu District, Guangzhou, China
[3]School of Civil and Transportation Engineering, Guangdong University of Technology, No. 100 Waihuangxi Road, Panyu District, Guangzhou, China

*Corresponding Author: Shaohua He. Email: hesh@gdut.edu.cn

Received: 16 January 2026; Accepted: 12 March 2026; Published: 30 June 2026

ABSTRACT: Ultra-high performance concrete (UHPC) exhibits exceptional mechanical properties and durability, making it highly suitable for infrastructure applications. This paper presents the design and evaluation of an innovative steel frame-UHPC composite deck intended for temporary trestles subjected to heavy construction loads and corrosive environments. The mechanical performance of the proposed composite deck was investigated through advanced finite element modeling and full-scale experimental testing. Structural responses of the trestle structure equipped with the composite deck under a 150-t crawler crane were analyzed numerically, while a three-point bending test on a full-scale steel frame-UHPC composite deck determined its flexural capacity and failure mechanisms. Stress distribution and deformation under bending loads were examined using calibrated numerical models and experimental data. Moreover, a parametric study was performed to assess the influence of key design variables. Results indicate that the steel frame-UHPC composite deck achieved an ultimate mid-span bending moment of 271.6 kN·m. Crack propagation in the UHPC panel of the composite deck was characterized by multiple, progressive cracks, demonstrating favorable ductility and early-warning capacity of the deck system. These findings confirm that the steel frame-UHPC composite deck offers high load-bearing capacity, flexural ductility, and favorable durability, supporting its use in heavy-duty trestle bridges and corrosive environments.

KEYWORDS: Trestle bridge; composite deck; steel frame; UHPC panel; mechanical performance

1 Introduction

The rapid development of transportation and municipal engineering has increased the demand for temporary and semi-permanent structures with enhanced performance. Construction trestle decks, as primary load-bearing components during bridge erection, are essential for ensuring safety, durability, and cost efficiency [1,2]. However, conventional trestle decks made of steel or normal concrete (NC) face significant challenges. Steel decks, while strong and lightweight, often generate excessive noise and are susceptible to corrosion, resulting in high maintenance costs [3,4]. NC decks, in contrast, have low tensile strength and high self-weight, which restrict span length and structural efficiency. Under repeated heavy loads, both types are prone to premature cracking and stiffness loss, compromising safety and service life [5–8]. The development of advanced trestle deck systems that integrate strength, toughness, durability, and economic viability remains a critical concern in modern bridge engineering.

Ultra-high performance concrete (UHPC) has recently received significant attention due to its outstanding compressive and tensile strengths, high toughness, and exceptional durability [9–13]. These superior properties have facilitated the wide adoption of UHPC in bridge deck constructions [14–18]. For example, Fayed et al. [19] investigated composite decks with a UHPC sub-layer and a NC top layer joined by steel connectors, demonstrating that UHPC-NC composite decks possess significantly higher ultimate resistance than conventional NC decks. Similarly, Shao et al. [20] developed a composite deck system incorporating UHPC panels with closely spaced ribs, resulting in reduced self-weight, increased sectional stiffness, and improved crack resistance. Despite these advancements, most existing studies have focused on solid UHPC decks for permanent bridges, and research on UHPC-based decks for temporary construction trestles is limited [21–24]. While UHPC deck solutions have the potential to address the shortcomings of traditional trestle decks, a systematic investigation of their failure mechanisms, modular design, and ability to withstand heavy construction equipment loads remains necessary.

This study introduces a novel trestle deck made from UHPC featuring a prefabricated modular design with a steel frame and hollow-panel configuration, specifically for temporary construction trestles. The hollow UHPC panel, which includes embedded multi-holes, enables lightweight construction while ensuring high load-bearing capacity, addressing the limitations of conventional steel and concrete decks. To investigate the failure mechanisms and ductility of the composite deck, the research involved numerical simulations and experimental tests. A 12 m-long construction trestle bridge with prefabricated steel frame-UHPC composite decks was modeled to evaluate structural responses under four loading scenarios from a 150-t crawler crane. Following this, a full-scale model test assessed load-deflection response, crack development, and ultimate load-bearing capacity. Based on these results, a validated nonlinear solid finite element (FE) model was developed, along with a parametric analysis exploring the effects of factors like material properties and structural configuration on performance. The findings provide a solid theoretical foundation and practical design guidelines for applying steel frame-UHPC composite decks in heavy-duty, port, and corrosive construction environments.

2 Numerical Simulation of Trestles with Steel Frame-UHPC Composite Decks

2.1 Background Construction Trestle Bridge

2.1.1 Arrangement and Configuration

As shown in Fig. 1, the background construction trestle consists of six prefabricated steel frame-UHPC composite decks positioned above ten standardized Bailey steel trusses. This assembly forms a simply supported beam structure with dimensions of 12.0 m in length, 8.0 m in width, and 1.5 m in depth, representative of temporary trestles commonly used in bridge erection projects. The 8.0 m deck width is selected to satisfy standard traffic requirements and ensure the unimpeded passage of construction vehicles. For example, a 150-t crawler crane has an outer edge distance of 7.1 m; thus, the 8.0 m-wide deck fully supports its track loads while maintaining an approximate 0.45 m margin on each side for guardrail installation. The substructure of Bailey steel trusses is fabricated from Q345 steel links and assembled with bolted connections, arranged beneath the composite decks. The prefabricated composite deck consists of a reinforced, multi-hole hollow UHPC panel with steel frames along the side edges. The steel frames are manufactured from standard Q345 steel channels, and the hollow panels are cast from UHPC with a target compressive strength of 120 MPa. Prefabricated UHPC panels are connected both to the Bailey steel trusses and to adjacent panels via steel bolts.

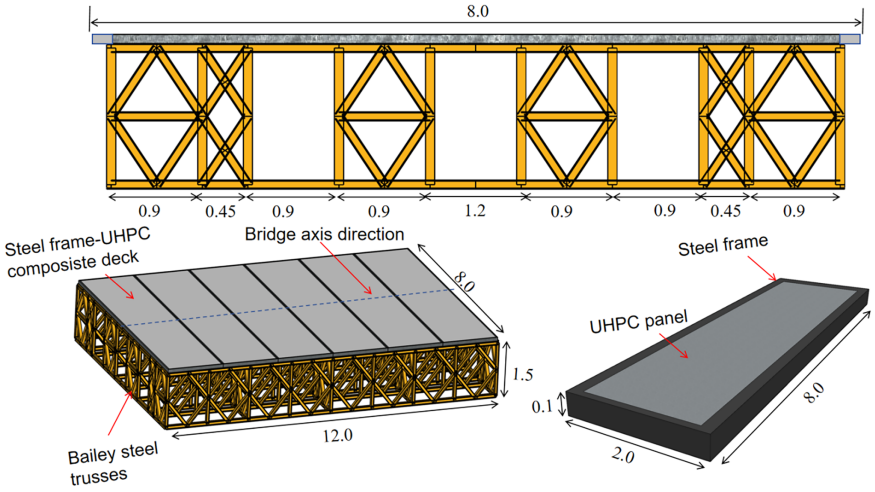

Figure 1: Arrangement and configuration of investigated trestle (Unit: m).

2.1.2 Details of Steel Frame-UHPC Composite Deck

Fig. 2 presents the details of the prefabricated steel frame-UHPC composite deck. The prefabricated composite deck measures 2.0 m in length, 8.0 m in width, and 0.1 m in thickness. The UHPC panel features several circular voids positioned at mid-height, each with a diameter of 34 mm and spaced at 33 mm intervals. Two layers of steel reinforcement are placed near the top and bottom edges of the holes. The longitudinal and transverse reinforcements have diameters of 8 and 10 mm, with spacing of 50 and 100 mm, respectively, and all reinforcements are of HRB400 grade. The concrete cover thickness is 17 mm on the top surface and 15 mm on the bottom. Steel frames are incorporated along the side edges of the UHPC panel, serving both as permanent formworks during concrete pouring and as lateral restraints. The total self-weight of a steel frame-UHPC composite deck is approximately 24 kN, which facilitates easy assembly during trestle construction.

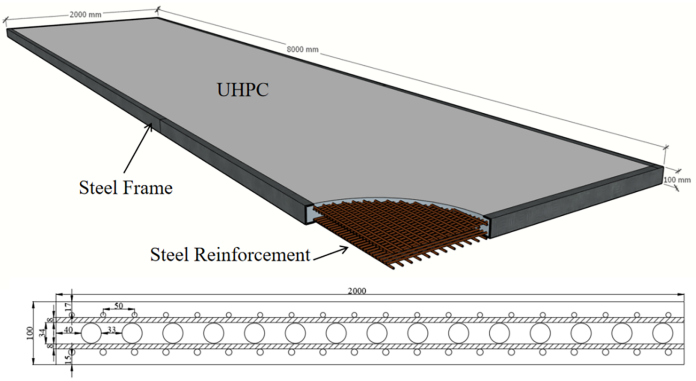

Figure 2: Configuration of steel frame-UHPC composite deck (Unit: mm).

2.2 Simulation of Trestle Structure

2.2.1 FE Model Establishment

A linear elastic FE model of the described trestle was developed utilizing MIDAS/CIVIL 2017, as shown in Fig. 3. The Bailey steel trusses were modeled using 1202 linear elastic link elements, while the composite deck panel was represented with 500 beam elements. The connections between the link and beam elements

were idealized as linear spring elements with a stiffness of 200 kN/mm, determined from bolt shear tests and in accordance with the Chinese design code GB 50017-2017 [25].

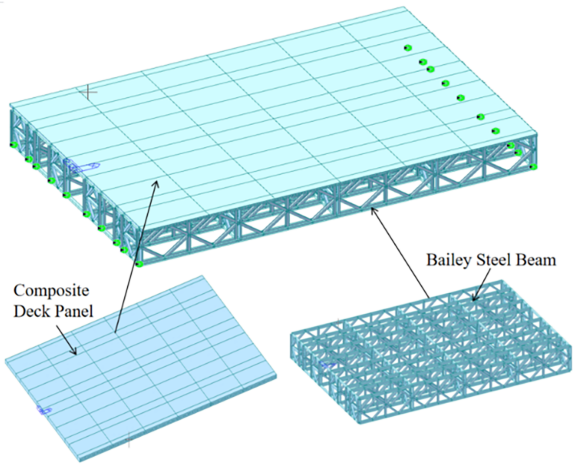

Figure 3: FE model of trestle with steel frame-UHPC composite deck.

The lengths of the link elements were established based on the actual dimensions of each steel truss, while the lengths of the beam elements for the UHPC panel were dictated by the connections between the UHPC panel and the Bailey steel trusses, as depicted in Fig. 1. The modeling approach adopted linear elastic representations for both the steel and UHPC materials. The mechanical properties of the materials are as follows: Q345 steel exhibits a yield strength of 386 MPa, an elastic modulus of 201 GPa, and a Poisson's ratio of 0.3. The HRB400 reinforcement possesses a yield strength of 408 MPa, an elastic modulus of 200 GPa, and a Poisson's ratio of 0.3. The UHPC demonstrates a compressive strength of 125 MPa and an elastic modulus of 45 GPa.

The global coordinate system was defined such that the x-, y-, and z-axes correspond to the length, width, and depth of the trestle, respectively. Simple support boundary conditions were implemented by restraining the nodes at one end of the trestle in the x, y, and z directions. At the opposite end, the nodes were restricted solely to the y and z directions, while rotational degrees of freedom were left unrestrained along all axes.

To assess the structural performance of the trestle system featuring the developed steel frame-UHPC composite deck, four representative loading scenarios were investigated using FE analysis. These scenarios were designed to capture the loading effects of a 150-t crawler crane, a typical piece of equipment in bridge construction. The crawler crane has an outer edge distance of 7.1 m, a track length of 7.0 m, and a track width of 0.2 m. As illustrated in Fig. 4, the crawler tracks are assumed to be positioned symmetrically relative to the bridge axis, with four composite deck panels in contact with the tracks. Load Case 1 models the crane in an unloaded configuration with a self-weight of 50 kN. Load Cases 2, 3, and 4 simulate the crane under full loading conditions, corresponding to a total weight of 1500 kN, with the boom oriented in the lateral, longitudinal, and most unfavorable directions, respectively. This comprehensive approach facilitates an evaluation of the trestle's behavior under critical construction loading conditions. The load was applied as uniformly distributed loads on the contact area between the crawler tracks and the composite deck, consistent with the actual stress state of the trestle during crane operation.

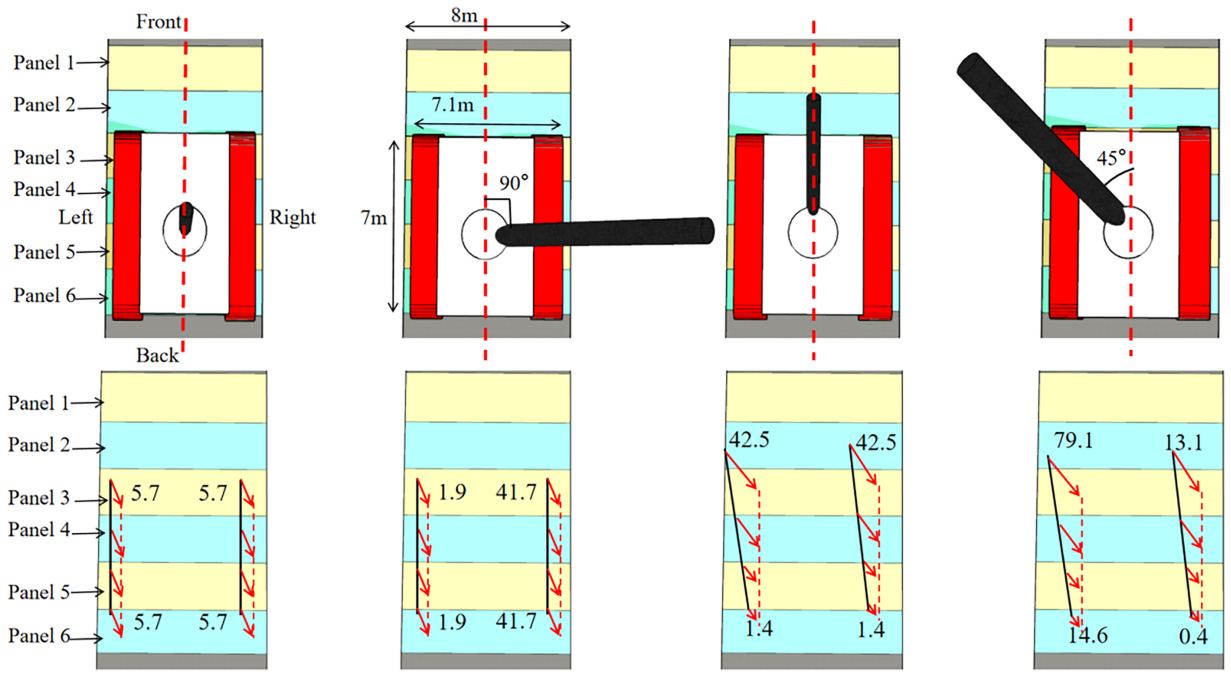

Figure 4: Schematic diagram of load cases (Unit: kN/m).

2.2.2 Result and Discussion

Table 1 presents a summary of the simulation results derived from the aforementioned trestle analytical models. Under all working conditions, the stresses in the steel frame-UHPC composite deck consistently remain within the allowable strength limits of the materials, ensuring the structural safety of the trestle under applied loads. The most critical scenario arises under Load Case 4, which results in a maximum bending moment of 146.8 kN·m, a maximum compressive stress of 44.9 MPa, a maximum tensile stress of 12.1 MPa, and a maximum deflection of 40.4 mm in the deck panel. It should be noted that the maximum tensile stress exceeds the allowable tensile stress of UHPC, which is attributed to the local stress concentration under the most unfavorable load direction; however, the steel reinforcement and steel frame in the composite deck can effectively bear the tensile force, preventing further crack development and structural failure.

Table 1: Simulation results.

	Bending Moment (kN·m)	Tensile Stress (MPa)	Compressive Stress (MPa)	Displacement (mm)
Case 1	16.3	2.7	4.9	6.1
Case 2	72.2	9.1	21.9	27.1
Case 3	111.5	11.4	34.1	24
Case 4	146.8	12.1	44.9	40.4

Fig. 5 presents the distributions of bending moment, nominal stress, and flexural displacement in the steel frame-UHPC composite decks under Load Case 4. An analysis in conjunction with Fig. 4 indicates that the most critical region of the UHPC panel for this load case is predominantly situated beneath the crawler track at the corner, while stresses in other regions of the panel remain consistently low. This observation implies that there is a sufficient safety margin for the overall integrity of the trestle structure. The

maximum deflection recorded under Load Case 4 is substantially below the permissible limit, confirming that the composite deck meets the stiffness criteria for temporary trestle applications. Moreover, the stress distribution within the steel frame is uniform, with no evidence of local buckling or significant stress concentrations. This finding further validates the effectiveness of the steel frame as a lateral restraint and load-bearing component.

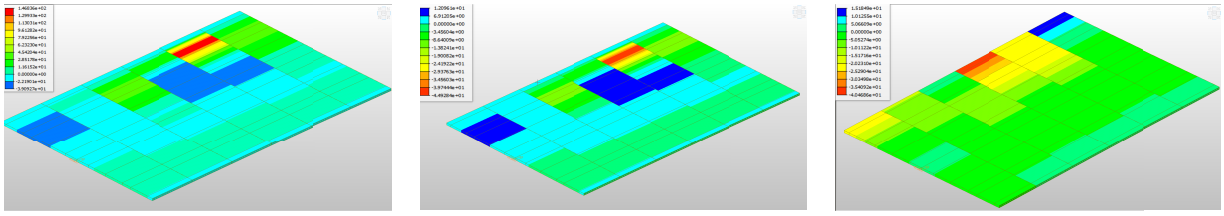

(**a**) (**b**) (**c**)

Figure 5: Simulation results for UHPC panel under Load Case 4 (**a**) bending moment; (**b**) stress; (**c**) displacement.

3 Model Test of Steel Frame-UHPC Composite Decks

3.1 Specimen Preparation

3.1.1 Materials

To examine the structural performance of the proposed steel frame-UHPC composite deck under critical loading conditions, a full-scale composite slab was fabricated according to the dimensions shown in Fig. 2. The UHPC employed in this experimental test was a commercially available mix, consisting of Portland cement (P·O 52.5R), silica fume (specific surface area ≥ 20,000 m^2/kg), quartz sand (particle size 0.1 to 0.6 mm), a polycarboxylate-based high-range water-reducing admixture (water reduction rate ≥ 30%), and straight steel fibers with a diameter of 0.2 mm and a length of 13 mm. The steel fiber volume fraction was 2%, and the water-binder ratio was 0.22. The 28-day compressive strength of standard cubes (100 mm × 100 mm × 100 mm) was measured at 125 MPa, with a corresponding cylinder compressive strength (100 mm × 200 mm) of 98 MPa and an elastic modulus of 45 GPa. Three standard specimens were tested for each properties to ensure data reliability, with the average value taken as the final result.

HRB400-grade steel reinforcement was utilized, featuring a nominal yield strength of 400 MPa and an elastic modulus of 200 GPa. Tensile tests were conducted on three reinforcement samples, yielding an average yield strength of 408 MPa and an ultimate tensile strength of 556 MPa. The steel frame was constructed from Q345 hot-rolled channel sections (10# channel steel), exhibiting a measured yield strength of 386 MPa, ultimate tensile strength of 510 MPa, and elastic modulus of 201 GPa. All material properties were tested in accordance with Chinese standard T/CECS 10107-2020 [26] and GB 50017-2017 [25], ensuring consistency with engineering practice.

3.1.2 Specimen Fabrication

Fig. 6 shows the specimen fabrication process. The slab was fabricated in a factory according to a standardized procedure to ensure dimensional accuracy and material uniformity. Initially, a steel frame was prepared by cutting and welding channel-shaped steel, with a 6 mm-thick flat steel plate used to assemble the bottom framework, thereby providing essential support during UHPC pouring. Subsequently, steel reinforcements and PE pipes, measuring 34 mm in diameter and 1 mm in wall thickness, were installed; the PE pipes were fixed at the mid-height of the formwork to ensure stability throughout the pouring process, while the steel reinforcements were bound according to the specified design spacing of 50 mm longitudinally

and 100 mm transversely, secured with tie wires. The PE pipes were retained after UHPC casting, as FE analysis indicated they had a negligible impact on the slab's flexural behavior. To prevent UHPC slurry from intruding during pouring, the ends of the PE pipes were sealed with foam rubber. Following this, UHPC was poured into the formwork, with a vibrating rod (30 mm diameter) at 2800 r/min applied to facilitate vibration compaction and eliminate internal voids. After the pour, the UHPC surface was covered with a plastic membrane to mitigate moisture loss. The curing process lasted 28 days under natural conditions, with regular water spraying to maintain moisture levels and ensure complete hydration of the UHPC before transportation to the laboratory for testing.

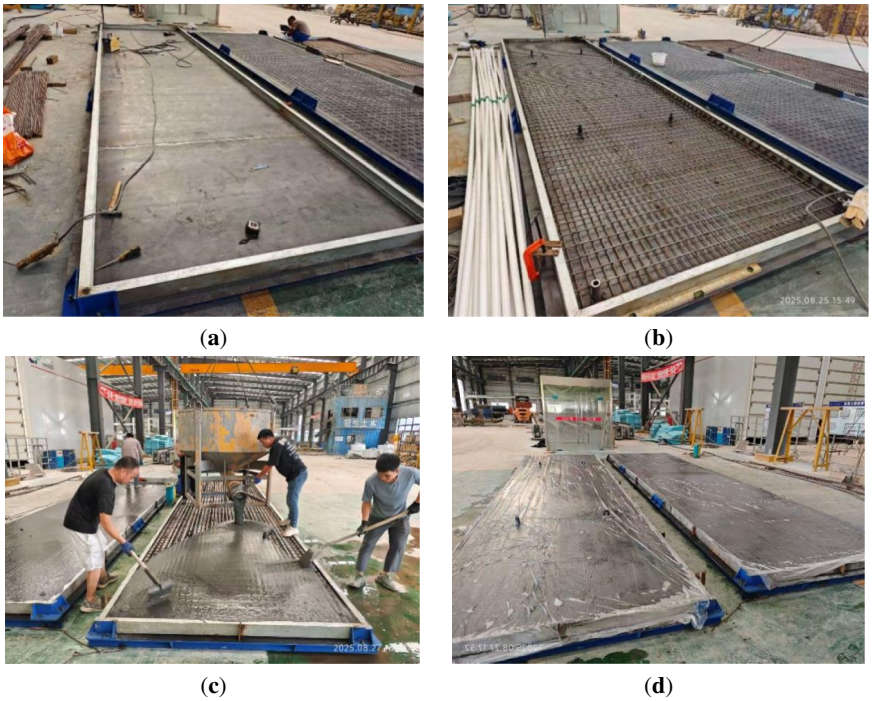

Figure 6: Illustration of specimen fabrication (**a**) fabrication of steel frame; (**b**) placement of reinforcement; (**c**) casting of UHPC; (**d**) curing process.

3.1.3 Loading Scheme

The fabricated steel frame-UHPC composite slab underwent testing using a three-point loading system, as shown in Fig. 7. The test setup included a rigid reaction frame, a 2000 kN hydraulic jack, and a load distribution beam to ensure uniform load application. A vertical load was applied via the hydraulic jack, which was connected to a displacement sensor to monitor the actuator's displacement.

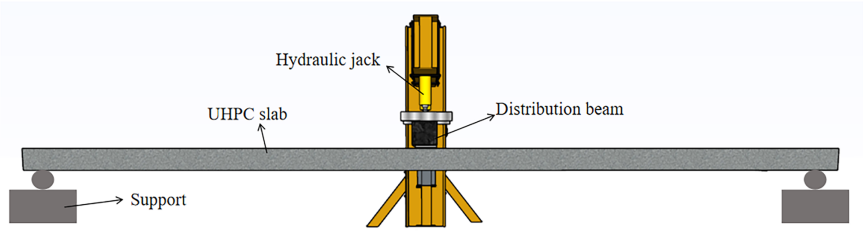

Figure 7: Test facilities arrangements.

The loading protocol employed a force-controlled mode during the elastic stage and a displacement-controlled mode during the post-yield stage. Before formal testing began, a preload of 20 kN was applied to verify that the test setup, instrumentation, and specimen connections were functioning properly. This preload was maintained for 5 min, after which the specimen was unloaded to zero to check for any initial deformation or instrument malfunctions.

During the main loading phase, a monotonic incremental loading protocol was used. In the elastic stage (before cracking), loads were increased in 10 kN increments at a rate of 0.2 kN/s, with each load level held for at least 1 min to allow for stable strain and displacement responses. If the slab developed severe cracks exceeding the allowable limit of 0.2 mm, or if significant non-linear mid-span deflection growth was observed, the loading mode was switched to displacement-controlled, with increments of 5 mm at a rate of 0.1 mm/s. The loading process continued until the slab experienced substantial damage. During this critical stage, each displacement increment was maintained for three minutes to monitor crack propagation and collect stable strain data.

3.1.4 Measurement Layout

Fig. 8 shows the instrumentation layout for the test slab, including detailed specifications of the measurement devices and their positions, ensuring clarity and reproducibility. The applied load from the hydraulic jack was measured using a force sensor located directly beneath it, which was calibrated prior to testing to ensure measurement accuracy. A total of eight concrete strain gauges were attached to the specimen: four gauges were affixed to the bottom surface at the L/4 span (two on each side of the mid-span, 20 cm from the slab edge), two gauges were placed on the bottom surface at the mid-span (evenly spaced along the width, 1.5 m apart), and two gauges were positioned on the top surface at the mid-span (corresponding to the bottom gauges). Additionally, three displacement transducers were installed on the bottom surface of the slab: one at the L/4 span, one at the mid-span, and one at the 3L/4 span, to accurately record vertical deflections. The Linear Variable Differential Transformers (LVDTs) were mounted on a rigid support frame independent of the test setup to prevent compliance of the measuring system.

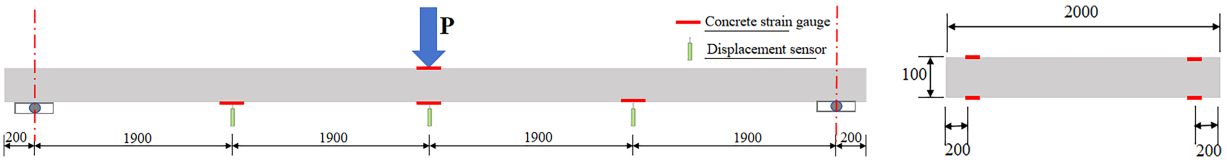

Figure 8: Measurement layout (Unit: mm).

3.2 Experimental Results

3.2.1 Failure Characteristics

Fig. 9 shows the failure state of the test slab. The UHPC slab exhibited ductile flexural failure, with local crushing in the compression zone at mid-span, yielding of the tensile reinforcement, and flexural yielding of the edge steel frame, all accompanied by audible failure sounds. The first fine crack appeared at the mid-span bottom at 28.1 kN, measuring 0.03 mm wide and accompanied by the sound of steel fibers being pulled from the matrix. As the load increased to 96 kN, this crack propagated laterally and reached the slab's top surface, while multiple fine cracks also developed on both sides of the primary crack. With loading up to 112 kN, the main crack widened to 2.1 mm and several additional flexural cracks formed at the slab bottom. At the ultimate load, the mid-span deflection reached 560 mm and the maximum compressive stress was 104 MPa. The substantial deflection of 560 mm is primarily due to the long composite deck's inherent

ductile failure mechanism, which allows significant post-yield deformation. The design of the hollow panel reduces its moment of inertia relative to that of a solid slab, thereby increasing deflection under ultimate loads. Additionally, the experimental setup facilitated minimal constraints on rotational deformation at the supports, contributing to the relatively large mid-span deflections under ultimate loads.

Figure 9: Failure mode diagrams: (**a**) overall bending and deflection of the UHPC slab; (**b**) compressive cracks at the top of the mid-span section; (**c**) cracks at the slab bottom edge; (**d**) primary crack at slab bottom.

3.2.2 Load-Deflection Curve

Fig. 10 presents the load-mid-span deflection response of the test slab, which demonstrates a distinct three-stage failure process, consistent with the failure characteristics observed.

Stage 1: Elastic Stage (0–28.1 kN): Extending from the onset of loading to the cracking load, the mid-span deflection exhibits an almost linear relationship with the applied load (correlation coefficient R^2 = 0.998), indicating stable flexural behavior. The slope of the curve corresponds to the initial bending stiffness (1434 kN/m), which is consistent with the theoretical calculation based on the section properties. During this stage, no cracks were observed, and both UHPC and steel were in the elastic state, with strains increasing linearly with load.

Stage 2: Elastoplastic Stage (28.1–112 kN): Spanning from steel yielding to imminent failure, this stage is characterized by a gradual reduction in flexural stiffness as the load increases, which is attributed to UHPC cracking, steel reinforcement yielding, and progressive damage to the UHPC matrix. The curve deviates from linearity, and the deflection growth rate accelerates. At the yield load of 96 kN, the mid-span deflection is 320 mm, and the tensile reinforcement begins to yield, transferring more load to the steel frame and UHPC compression zone. During this stage, cracks propagate and widen, but the structure remains capable of bearing additional load due to the ductility of steel and UHPC.

Stage 3: Failure Stage: A rapid escalation in mid-span deflection is observed, accompanied by the propagation and widening of cracks, crushing of the UHPC in the compression zone, yielding of the internal reinforcement, and eventual loss of load-carrying capacity. The load decreases gradually as the specimen undergoes significant plastic deformation, and the deflection increases to 650 mm when the load drops to 80% of P_u. This staged response provides clear insight into the structural performance and failure mechanisms of the UHPC composite slab under flexural loading, confirming its ductile behavior and safety margin.

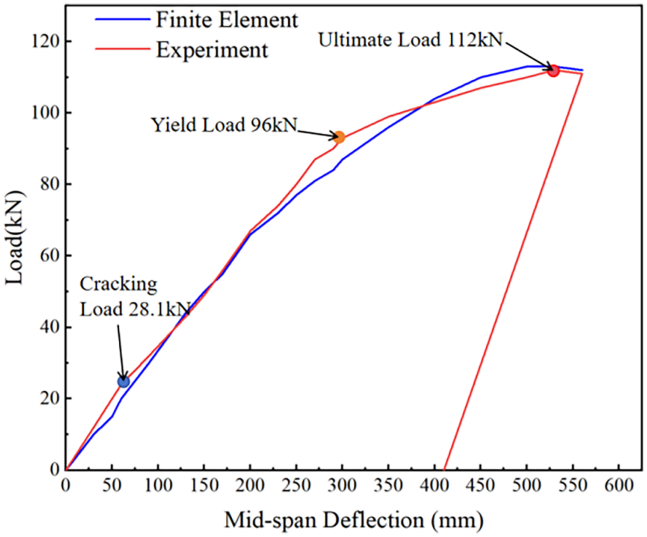

Figure 10: Load vs. mid-span deflection curve.

3.2.3 Strain History of UHPC Panel

Fig. 11 presents the load-strain relationship for the UHPC panel, highlighting the distinct responses occurring before and after the cracking load of 28.1 kN. Prior to reaching this critical threshold, both tensile and compressive strains show a nearly linear increase with the applied load, which demonstrates the elastic behavior of the UHPC panel (R^2 = 0.996 for tensile strain and R^2 = 0.997 for compressive strain). At the cracking load, the tensile strain at the mid-span bottom of the panel peaks at 205 με, consistent with the expected tensile capacity of UHPC, thereby confirming the initiation of cracking. When the load reaches approximately 28.1 kN, the tensile strain peaks and then decreases sharply, coinciding with the appearance of visible cracks at the mid-span bottom. This indicates that the UHPC in the tensile zone can no longer support loads, necessitating reliance on the steel reinforcement as the primary tensile component.

In contrast, the compressive strain continues to rise steadily, as the UHPC in the compression zone remains intact and effectively bears the compressive load. Upon further loading up to 96 kN, the compressive strain gradually increases, reaching around 1200 με at the yield load. Beyond this yield point, the compressive strain rises rapidly, indicating the progressive yielding of the reinforcement. At the ultimate load, the compressive strain at the mid-span top exceeds the UHPC's ultimate compressive strain capacity, indicating local crushing. This sequenced response elucidates the structural performance and failure mechanisms under flexural loading, aligning with the observed load-deflection curve and the various failure modes identified in the study.

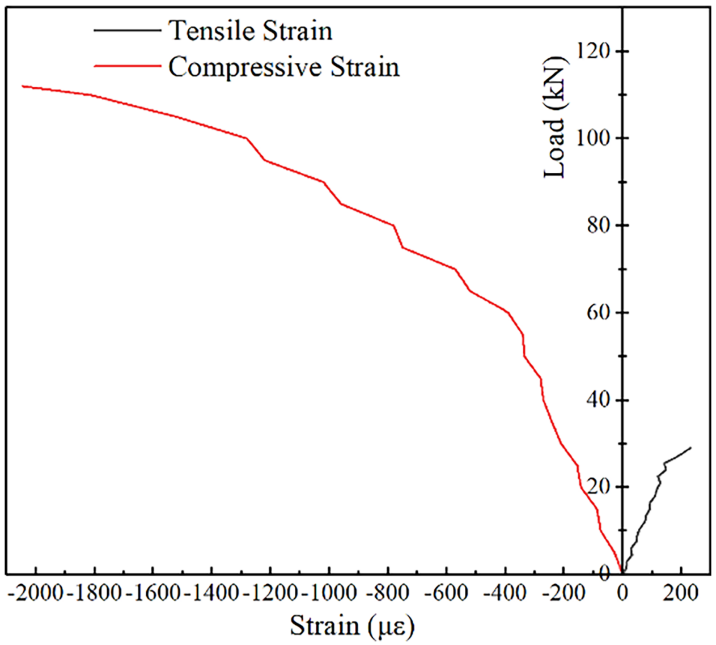

Figure 11: Load vs. mid-span strain curve of UHPC panel.

4 Parametric Analysis of Steel Frame-UHPC Composite Deck

4.1 Establishment of FE Solid Model

A solid FE model was developed using ANSYS 2022 to identify critical design parameters for the composite deck. The model's coordinate system was defined with the x-axis at 8 m (width), the y-axis at 2 m (length), and the z-axis at 0.1 m (thickness). UHPC was modeled using Solid 65 elements, channel steel with Shell 188 elements, and steel reinforcements with Link 8 elements. A mesh size of 40 mm was chosen based on a sensitivity study, which showed a maximum deviation of less than 2.5% in ultimate load between 30 and 40 mm, ensuring a balance between computational efficiency and accuracy. The solid FE model of the steel frame-UHPC composite deck is established as shown in Fig. 12.

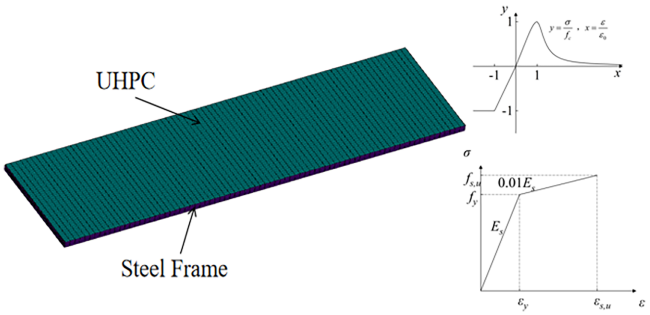

Figure 12: Solid model of steel frame-UHPC composite deck.

The interface between the UHPC and steel was modeled with a coupling constraint. The axial behavior of UHPC in tension and compression was evaluated using the methodologies of Naeimi and Moustafa [27] and Savino et al. [28], respectively, with ε_0 denoting the peak strain corresponding to the compressive strength (f_c). The UHPC's compressive strength was established at 125 MPa with a peak strain of 3800 με, while

tensile softening was calibrated using experimental cracking data, adjusting the fracture energy to 125 N/m. The uniaxial tension behavior of steel was represented by a bilinear model, incorporating a strain hardening modulus of 20 GPa based on tensile tests of Q345 steel and HRB400 reinforcement. The rest parameters for the material constitutive model were determined based on the experimental results described above.

Displacement constraints were implemented to mirror the three-point loading test setup, with D_y and D_z restrained on the left support and D_x, D_y, and D_z restrained on the right. A concentrated mid-span load was applied incrementally to simulate monotonic loading, aligning with the experimental configuration.

4.2 Validation of FE Model

Fig. 13 presents the damage pattern of the slab in its ultimate state. As evident, the cracking distribution and ultimate failure characteristics predicted by the FE model closely mirror those observed in the experimental test, showcasing numerous laterally spreading cracks on the UHPC surfaces, along with the yielding of both the tensile reinforcement and edge steel frames. The maximum stresses recorded in the UHPC and steel, as derived from the FE model, are approximately 107.2 and 400 MPa, respectively. These values align with the material's compressive strength limit and are consistent with experimental observations, which indicated localized crushing in the compression zone and yielding of the steel components.

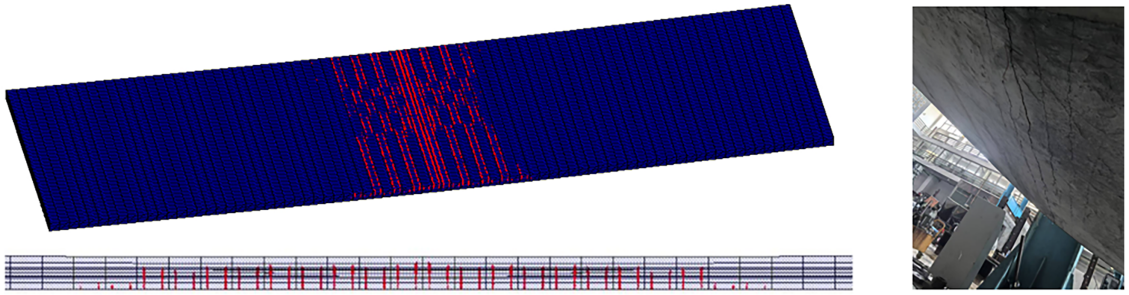

Figure 13: UHPC panel crack diagram.

Table 2 presents a comparison of the numerical and experimental results. In this table, K represents the bending stiffness; P_{cr} is the initial cracking load; δ_{cr} denotes the mid-span deflection at P_{cr}; P_u is the ultimate load; M_u corresponds to the maximum bending moment at P_u; and δ_u is the maximum mid-span deflection. The results calculated from the established FE model are in close agreement with the experimental data, with an average relative error of 6.1%. This outcome demonstrates the reliability of the finite element simulation. However, the prediction error for the ultimate displacement is significantly higher, reaching 18.3%. Several factors can explain this discrepancy. Firstly, the numerical model assumed an ideal bond between the UHPC panel and the steel frame. However, in the experimental specimen, some minor interface slip likely occurred, resulting in a higher actual displacement. Additionally, the FE model did not account for damage to the PE pipe interfaces used to create voids within the UHPC panel, which may have contributed to the additional deformation observed in the experiment. Lastly, the constitutive model for UHPC used in the numerical simulation failed to accurately capture post-crushing behavior, resulting in an underestimation of the residual deformation.

Table 2: Mechanical properties of steel frame-UHPC composite deck.

Series	K (kN/m)	P_{cr} (kN)	δ_{cr} (mm)	P_u (kN)	M_u (kN·m)	δ_u (mm)
Experimental test	1434	28.1	19.6	112	271.6	560
Numerical simulation	1373	27.6	20.1	118.5	282.1	457.3
Relative error (%)	4.2	1.8	2.6	5.8	3.9	18.3

4.3 Assessment of Design Parameters

Based on the validated FE model, a parametric study was conducted to identify the key design parameters for the developed steel frame-UHPC composite deck. The parameters evaluated in this section include the thickness of the UHPC panel (80, 100, and 150 mm), the reinforcement ratio of the UHPC panel (0.5%, 1.0%, and 1.3%), the plate thickness of the steel frame (4, 6, and 8 mm), and the compressive strength of UHPC (120, 140, and 160 MPa).

4.3.1 Influence of UHPC Panel Thickness

The thickness of the UHPC panel is a critical parameter affecting the flexural performance of the composite deck. Fig. 14 shows the influence of UHPC panel thickness on the flexural properties of the deck. It is evident that the use of a thicker UHPC panel results in higher cracking load, yield load, and ultimate resistance for the steel frame-UHPC composite deck. Specifically, increasing the panel thickness from 80 to 150 mm enhances the cracking, yield, and ultimate loads by 41.3%, 108.3%, and 96.6%, respectively. These improvements can be attributed to the direct increase in the sectional moment of inertia and the height of the compression zone caused by a thicker UHPC panel, thereby improving the bending resistance of the section. Furthermore, a thicker UHPC slab distributes loads more effectively, delays crack propagation, and improves structural ductility. In contrast, reducing the slab thickness results in a significant decrease in sectional stiffness and an insufficient compression zone area, making the section susceptible to early crushing and reducing the load-bearing capacity.

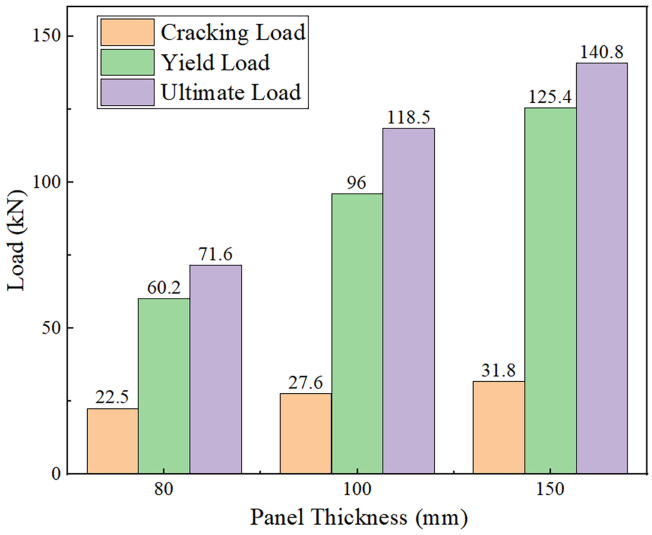

Figure 14: Influence of UHPC panel thickness.

4.3.2 Influence of Longitudinal Reinforcement Ratio

Fig. 15 plots the flexural performance of steel frame-UHPC composite decks with reinforcement ratios varying from 0.5% to 1.3%. It is observed that an increase in the longitudinal reinforcement within the UHPC panel does not substantially influence the cracking load of the composite deck. Nonetheless, significant enhancements are observed in both the yield and ultimate load capacities. Specifically, relative to the panel with a 0.5% reinforcement ratio, the yield loads for panels with reinforcement ratios of 1.0% and 1.3% are elevated by 72% and 106.4%, respectively, while the corresponding increases in ultimate resistance reach 80.3% and 118.2%, respectively. These results are consistent with theoretical expectations, as an increased reinforcement ratio expands the total area of tensile steel bars, thereby augmenting the tensile force capacity at yield and improving the section's flexural resistance. Moreover, insufficient reinforcement ratios diminish the crack-bridging capacity of the steel bars, leading to more rapid crack width development, reduced structural ductility, and an increased propensity for brittle failure.

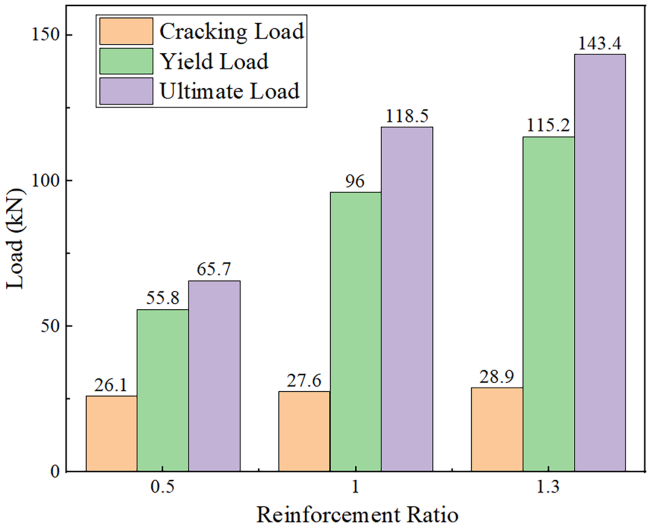

Figure 15: Influence of reinforcement ratio.

4.3.3 Influence of Steel Frame Thickness

Serving as the edge restraint in the steel frame-UHPC composite deck, the steel frame plays a crucial role in maintaining the integrity, local stability, and torsional performance of the composite deck system. A reduction in the steel frame thickness may diminish the effectiveness of composite action between the UHPC panel and steel frame, potentially resulting in local buckling. Fig. 16 compares the flexural properties of composite decks with varying steel frame plate thicknesses. It is evident that increasing the plate thickness enhances the flexural performance of the composite decks. Compared to the deck utilizing a 4 mm-thick steel plate, the cracking, yield, and ultimate loads of the deck with a 6 mm-thick plate increased by 3%, 4.2%, and 8.1%, respectively. Further increasing the plate thickness to 8 mm resulted in improvements of 5.6% in cracking load, 5.9% in yield load, and 12.6% in ultimate load. Increasing the steel frame thickness enhances the local stiffness at the section edges, strengthens the cooperative action between the UHPC slab and steel frame, and facilitates more effective load transfer and distribution.

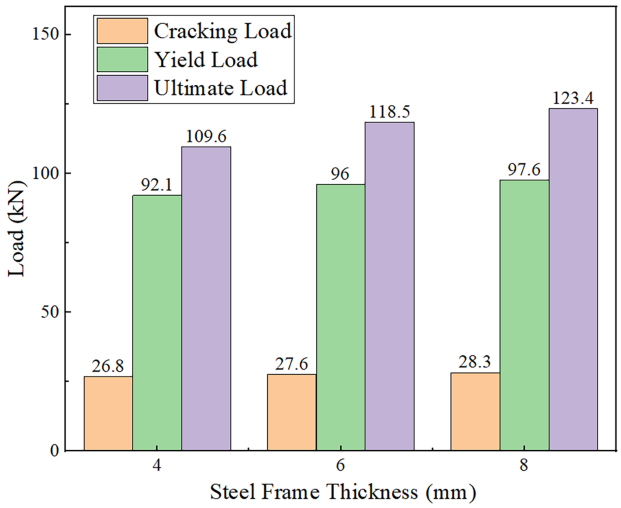

Figure 16: Influence of steel frame thickness.

4.3.4 Influence of UHPC Strength

Fig. 17 shows the mechanical properties of composite decks with varying UHPC compressive strengths. As shown, increasing UHPC strength results in a steady increase in the composite deck's cracking, yield, and ultimate loads. Specifically, decks with a UHPC strength of 140 MPa exhibited increases of 5.8%, 2.6%, and 3.6% in cracking, yield, and ultimate loads, respectively, compared to those with a strength of 120 MPa. Furthermore, when a 160 MPa UHPC was used, these improvements reached 11.6%, 6.4%, and 7.2%, respectively. This enhanced load-bearing capacity can be attributed to the high strength of UHPC, which improves the compression zone of the UHPC panel, thereby delaying crushing and enhancing crack resistance. However, it is important to note that since the composite structure predominantly depends on steel reinforcement and frames to handle the main tensile forces, the contribution of increased UHPC strength to overall load capacity is significantly less than that of panel thickness and reinforcement ratio, serving more as an auxiliary improvement.

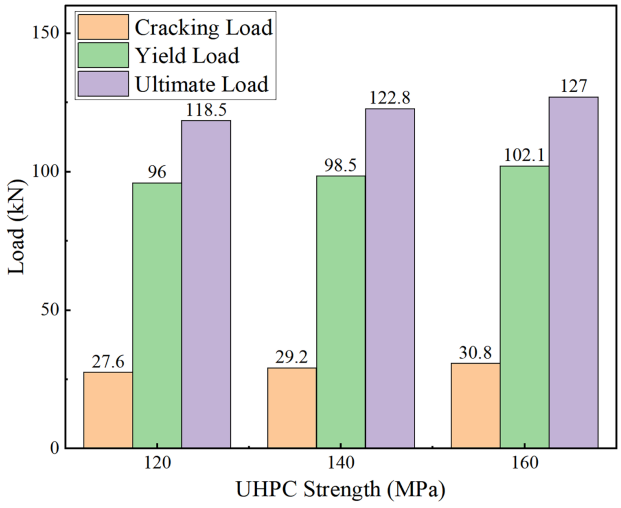

Figure 17: Influence of UHPC strength.

Simulation results indicate that slab thickness exerts the greatest effect on ultimate bearing capacity, with a 50 mm (50%) increase yielding an 18.8% improvement. The reinforcement ratio is also critical; halving it results in a 44.6% reduction in ultimate bending capacity, underscoring the importance of adequate longitudinal steel reinforcements. In contrast, steel frame thickness has a minimal impact, with a 33% change causing only a 7.5% variation. The steel frame primarily provides structural support and connectivity rather than directly contributing to load-bearing capacity. Since the UHPC slab primarily relies on steel reinforcement and the steel frame to bear tensile forces, the UHPC strength has a limited effect on enhancing the load-bearing capacity.

5 Design and Application Recommendations

Based on a thorough analysis of experimental and numerical findings, engineering design and application recommendations for the studied composite deck are suggested. The initial step is to determine the design load by assessing the impact of construction equipment, such as a 150-t crawler crane. It is crucial to quantify the maximum bending moment and shear force exerted on the composite deck using the FE simulation methodology.

In terms of material selection, the study recommends UHPC with specified properties: a minimum compressive strength of 120 MPa and a fracture energy threshold of at least 100 N/m. Such specifications are crucial for achieving the necessary load-bearing capacity and ductility. Regarding structural dimensions, for standard 2.0 m-span trestle decks, a slab thickness of 100 to 120 mm is recommended to balance weight and load-carrying capacity effectively. For applications involving heavier loads, for example, higher than 200 t, an increased slab thickness of 150 mm is advised.

A longitudinal reinforcement ratio of 1.0% to 1.2% using HRB400 grade steel is recommended to ensure adequate tensile strength and ductility. To prevent brittle failure, a minimum reinforcement ratio of 0.8% is necessary. Additionally, the channel steel frame thickness should be evaluated, with a recommendation of 6 to 8 mm for steel plates made of Q345 material, to ensure sufficient lateral restraint and effective composite behavior between the UHPC panel and the steel framework. The design's safety margins must be meticulously verified to ensure that the maximum stresses in both UHPC and steel remain within permissible limits.

6 Conclusion

To address the challenges posed by heavy construction loads and corrosive environments in temporary construction trestles, this study introduces an innovative steel frame-UHPC composite deck. By integrating numerical simulation, full-scale experimental testing, and parametric analysis, the research evaluates the failure performance and effects of critical design parameters of the composite deck. The principal findings are summarized as follows:

(1) The steel frame-UHPC composite deck demonstrates outstanding load-bearing and deformation capacity. Full-scale three-point bending tests reveal an ultimate mid-span bending moment of 271.6 kN·m and a mid-span deflection of 560 mm, indicative of ductile flexural failure. Progressive cracking in the UHPC panel, as opposed to abrupt brittle failure, confers favorable early-warning characteristics for structural safety.

(2) Panel thickness (80 to 150 mm) and reinforcement ratio (0.5% to 1.3%) are the primary determinants of ultimate load-bearing capacity. A 50% increase in panel thickness improves capacity by 18.8%, while halving it reduces capacity by 39.6%. Likewise, halving the reinforcement ratio decreases capacity by 44.6%, whereas a 30% increase raises it by 21%. In contrast, steel frame thickness (4 to 8 mm) has a negligible effect, causing only a 7.5% variation in capacity and serving mainly as a constraint and connection element.

(3) The steel frame-UHPC composite deck synergistically integrates the advantages of steel and UHPC, achieving high load-bearing capacity, ductility, and promising durability potential. Its prefabricated, modular design results in a self-weight of only 24 kN, facilitating rapid construction and assembly. This system is well-suited to demanding environments involving heavy loads and corrosion, offering a promising solution for temporary construction trestles and related applications.
(4) Although the developed steel frame-UHPC composite deck offers significant advantages in static bending performance in the present study, the punching shear properties under heavy crawler crane and the fatigue performance of the composite deck are recommended in future research.

Acknowledgement: Not applicable.

Funding Statement: The National Natural Science Foundation of China (Grant # 52278161).

Author Contributions: The authors confirm contribution to the paper as follows: writing—original draft preparation, investigation, Wu Yang; writing—original draft preparation, data curation, conceptualization, Quan Xu; methodology, validation, resources, data curation, Zhimin Zhou; conceptualization, validation, Mingtao Ye; funding acquisition, supervision, visualization preparation, writing—review & editing, Shaohua He. All authors reviewed and approved the final version of the manuscript.

Availability of Data and Materials: The data that support the findings of this study are available from the corresponding author upon reasonable request.

Ethics Approval: Not applicable.

Conflicts of Interest: The authors declare no conflicts of interest.

References

1. Nowak AS, Eamon CD. Reliability analysis of plank decks. J Bridge Eng. 2008;14(5):540–6. doi:10.1061/(ASCE)1084-0702(2008)13:5(540).
2. Wang ZX, Su K, Huang Y, Zhou CD. Construction technology of steel structure hoisting under the pier deck of a certain project. Build Technol Dev. 2025;52(2):12–4. doi:10.20259/j.jzjskf.2025.02.0012. (In Chinese).
3. Yamada T, Shinoda N, Takeuchi K, Masaki M. Development of automatic steel deck cutting system using a multi-axis robot for power plant construction work. Int Conf Comput Civ Build Eng. 2025;629(4):383–97. doi:10.1007/978-3-031-87364-5_32.
4. John K, Ashraf M, Weiss M, Al-Ameri R. Experimental and finite element study of a novel two-way corrugated steel deck system for composite slabs. J Compos Sci. 2022;6(9):261. doi:10.3390/jcs6090261.
5. Lecieux Y, Rozière E, Gaillard V, Lupi C, Leduc D, Priou J, et al. Monitoring of a reinforced concrete wharf using structural health monitoring system and material testing. J Mar Sci Eng. 2019;7(4):84. doi:10.3390/jmse7040084.
6. Rodriguez-Ocampo PE, Fontes JVH, Ring MC, Mendoza E, Esperanca PTT, Silva R. Evaluation of the influence of deck slope on green water loads using the wet dam-break approach. J Braz Soc Mech Sci Eng. 2024;46(1):42. doi:10.1007/s40430-023-04611-1.
7. Ibrahim A, Abdelkhalek S, Zayed T, Qureshi AH, Mohammed Abdelkader E. A comprehensive review of the key deterioration factors of concrete bridge decks. Buildings. 2024;14(11):3425. doi:10.3390/buildings14113425.
8. Degtyarev VV. Concent load distribution in corrugated steel decks: a parametric finite element study. Eng Struct. 2020;206(2–3):110158. doi:10.1016/j.engstruct.2019.110158.
9. He S, Huang X, Zhong H, Wan Z, Liu G, Xin H, et al. Experimental study on bond performance of UHPC-to-NC interfaces: constitutive model and size effect. Eng Struct. 2024;317(S1):118681. doi:10.1016/j.engstruct.2024.118681.
10. Jin W, Yang Q, Peng X, Xu B. A review on mechanism and influencing factors of shear performance of UHPC beams. Buildings. 2024;14(11):3351. doi:10.3390/buildings14113351.

11. Xiao G, Chen X, Xu L, Kuang F, He S. Flexural performance of UHPC-reinforced concrete T-beams: experimental and numerical investigations. Struct Durab Health Monit. 2025;19(5):1167–81. doi:10.32604/sdhm.2025.064450.
12. Zhong H, Chen Z, Liu C, He S, Wan Z, Yu Z. Fatigue shear failure mechanism and prediction method for UHPC-NC bond interfaces. Eng Struct. 2025;336(3):120455. doi:10.1016/j.engstruct.2025.120455.
13. Anunike GS, Tarabin M, Hisseine OA. Assessment of the mechanical, radiation shielding, and durability of ultra-high-performance concrete for radiation shielding: a review. Constr Build Mater. 2025;474(2–3):140896. doi:10.1016/j.conbuildmat.2025.140896.
14. Kravanja G, Mumtaz AR, Kravanja S. A comprehensive review of the advances, manufacturing, properties, innovations, environmental impact and applications of ultra-high-performance concrete (UHPC). Buildings. 2024;14(2):382. doi:10.3390/buildings14020382.
15. Xu R, Li J, Li W, Zhang W. Experimental and numerical study of bonding capacity of interface between ultra-high performance concrete and steel tube. Struct Durab Health Monit. 2025;19(2):285–305. doi:10.32604/sdhm.2024.057513.
16. Peng G, Wu J, Shi C, Hu X, Niu D. Effect of thermal curing regimes on the mechanical properties, and durability of UHPC: a state-of-the-art review. Structures. 2025;74(3):108667. doi:10.1016/j.istruc.2025.108667.
17. Redžić N, Grgić N, Baloević G. A review on the behavior of ultra-high-performance concrete (UHPC) under long-term loads. Buildings. 2025;15(4):571. doi:10.3390/buildings15040571.
18. Shokrgozar A, Aryal B, Ebrahimpour A, Mashal M. Bond-silp behavior of steel reinforcing bars in ultra-high performance concrete for field-cast connection of precast bridge decks. Front Built Environ. 2024;10:1354657. doi:10.3389/fbuil.2024.1354657.
19. Fayed S, Madenci E, Özkiliç YO, Basha A. The flexural behaviour of multi-layered steel fiber reinforced or ultra-high performance-normal concrete composite ground slabs. J Build Eng. 2024;95(6):109901. doi:10.1016/j.jobe.2024.109901.
20. Shao X, Yi D, Huang Z, Zhao H, Chen B, Liu M. Basic performance of the composite deck system composed of orthotropic steel deck and ultrathin RPC layer. J Bridge Eng. 2013;18(5):417–28. doi:10.1061/(asce)be.1943-5592.0000348.
21. Qiu M, Shao X, Yan B, Zhu Y, Chen Y. Flexural behavior of UHPC joints for precast UHPC deck slabs. Eng Struct. 2022;251(2):113422. doi:10.1016/j.engstruct.2021.113422.
22. Wan Z, Fang Z, Liang L, He S, Sun X. Structural performance of steel-concrete composite beams with UHPC overlays under hogging moment. Eng Struct. 2022;270(11):114866. doi:10.1016/j.engstruct.2022.114866.
23. Zhou M, Lu W, Song J, Lee GC. Application of ultra-high performance concrete in bridge engineering. Constr Build Mater. 2018;186(7):1256–67. doi:10.1016/j.conbuildmat.2018.08.036.
24. He S, Huang X, Zou L, Zheng C, Xin H, Liang J. Performance assessment of channel beam bridges with hollow track bed decks. Structures. 2024;61(2):105988. doi:10.1016/j.istruc.2024.105988.
25. GB 50017-2017. Standard for design of steel structures. Beijing, China: Ministry of Housing and Urban-Rural Development of the People's Republic of China; 2017. (In Chinese).
26. T/CECS 10107-2020. Technical requirements for ultra high performance concrete. Beijing, China: China Association for Engineering Construction Standardization; 2020. (In Chinese).
27. Naeimi N, Moustafa MA. Compressive behavior and stress-strain relationships of confined and unconfined UHPC. Constr Build Mater. 2021;272(9):121844. doi:10.1016/j.conbuildmat.2020.121844.
28. Savino V, Lanzoni L, Tarantino AM, Viviani M. Tensile constitutive behavior of high and ultra-high performance fibre-reinforced-concretes. Constr Build Mater. 2018;186(8):525–36. doi:10.1016/j.conbuildmat.2018.07.099.